Talanta 250 (2022) 123688

Contents lists available at ScienceDirect

Talanta

journal homepage: www.elsevier.com/locate/talanta

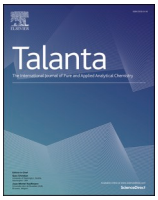

Chromatographic framework for coffee ring effect-driven separation of small molecules in surface enhanced Raman spectroscopy analysis

Valery Liamtsau [a], Guangliang Liu [a], Alexander N. Morozov [a], Alexander M. Mebel [a], Yong Cai [a,b,*]

[a] Department of Chemistry and Biochemistry, Florida International University, Miami, 11200 SW 8th ST, Miami, FL 33199, USA
[b] Southwest Environmental Research Center, Florida International University, 11200 SW 8th ST, Miami, FL 33199, USA

ARTICLE INFO

Keywords:
Coffee ring effect
Gold nanofilm
Raman spectroscopy
Arsenic
Nanochromatography
Separation

ABSTRACT

The applications of coffee ring effect (CRE) in analytical chemistry have been increasingly expanded from particles and macromolecules to small molecules, in particular coupled to surface-enhanced Raman spectroscopy (SERS). Despite the theory behind the formation of CRE itself from a single drop evaporation onto the dry surface is well established, the theoretical aspects of CRE-driven separation, especially the analyte-surface interactions involving small molecules, have not been conceived. Herein, we have developed a theoretical framework to describe the CRE-driven separation process of small molecules, using SERS analysis of dimethylarsinic acid (DMA^V), dimethylmonothioarsinic acid ($DMMTA^V$), and dimethyldithioarsinic acid ($DMDTA^V$) on gold nanofilm (AuNF) as an example. By combining the CRE theory for the radial flow and the Extended Derjaguin-Landau-Verwey-Overbeek (XDLVO) theory for mass transfer between solution and AuNF surface, we adapted the conventional chromatographic theory to derive a modified van Deemter equation for the CRE-driven separation. By using this model, we predicted the travel distances of arsenicals based on the different affinity of analytes to the AuNF and evaluated the possibility of separation of unknown analytes by CRE-based SERS, demonstrating the successful adaptation of classic chromatographic theory to CRE-driven nanochromatography.

1. Introduction

The evaporation process of a sessile droplet containing suspended or nonvolatile particles normally leads to a ring-shaped formation on a flat substrate. These stains are produced by the so-called coffee ring effect (CRE) that has been firstly explored by Deegan et al. [1], where the author described the transport of solid particles to the edge of the drying droplet during the solvent evaporation. To replenish the solvent loss at the three-phase contact line, the radial outward flow was generated from the center to the edge regions of the evaporating droplet [1–3]. The major application of CRE was commonly attributed to the enrichment of nanoparticles and macromolecules in the ring region by coupling CRE with fluorescence [4], matrix-assisted laser desorption [5] and Raman spectroscopy [6], enabling a relatively low limit of detection of polymeric nanocrystals [7], proteins [8], and polycyclic aromatic hydrocarbons [9]. Typically, CRE driven particles deposition begins once the radial flow starts bringing the droplet solution to the edge of the three-phase contact line simultaneously carrying colloidal particles away from the center region resulting in their accumulation at the forming ring stain [10].

In addition to the particle's enrichment, the radial flow found its applications in the separation of the micro- and nanoparticles based on their size variation. In these applications the separation capability of the CRE was based on the size differences in particles or molecules. Generally, the larger the molecular size, the lesser the influence of the radial outward flow and thus, the molecule would travel a shorter distance. This approach was applied for the separation of IgG antibodies and *E-Coli* cells [11], silicon nanocrystals [7], platinum nanoclusters [5], polystyrene bids [7], silica microparticles [12], and nanorods polymer monoliths [13].

The separation capability of the CRE was further exploited for small molecules, albeit challenging and in a limited number of studies. It is of particular interest to couple the CRE with surface-enhanced Raman spectroscopy (SERS), as this provides an approach that does not require a major sample preparation and allows simultaneous detection of analytes thanks to their separation by CRE and distinct vibrational

* Corresponding author. Department of Chemistry and Biochemistry, Florida International University, Miami, 11200 SW 8th ST, Miami, FL 33199, USA.
E-mail address: cai@fiu.edu (Y. Cai).

https://doi.org/10.1016/j.talanta.2022.123688
Received 21 February 2022; Received in revised form 9 June 2022; Accepted 11 June 2022
Available online 18 June 2022

fingerprints [14]. In SERS, the propagation of surface plasmons electromagnetic waves, through electromagnetic and chemical enhancement mechanisms, could enable amplification of the inherently weak Raman signal by providing an increased electric field in the vicinity of the target molecule and the nanomaterial [15]. The fabrication of SERS-active substrates and the preconcentration of analytes could be integrated into one step, as previously demonstrated [16]. The nanofilm surface can be used not only for the separation of analytes but also for the Raman signal enhancement. In previous studies, we have applied CRE coupled with SERS on the silver nanofilm for the speciation of stable oxoarsenic species (As^{III}, As^{V}, DMA^{V}, MMA^{V}) [17] and unstable thioarsenicals (dimethylmonothioarsinic acid, $DMMTA^{V}$ and dimethyldithioarsinic acid $DMDTA^{V}$) onto the gold nanofilm (AuNF) [18]. Manipulating the chemical environment (e.g., pH and buffer solution) enabled us to control the traveled distances of the arsenicals across the drying droplet, aiding in their identification besides their distinct Raman shifts. Indeed, the selective deprotonation of target compounds induces the unique interactions of molecules with the AuNF surface resulting in their distinct traveled distances. Besides, the hydroxyl of DMA^{V}, thiol of $DMDTA^{V}$, and thionyl of $DMMTA^{V}$ functional groups have a different affinity to the AuNF surface, leading to specific interactions with AuNF, controlling their adsorption on the surface and traveled distances during the formation of the coffee ring stain. Eventually, the molecular charge and the chemical composition of individual arsenicals enabled us to predict the deposition of each molecule at the specific region across the coffee ring deposit.

The expanded applications of CRE-driven separation from particles to macromolecules and small molecules prompt us to consider the theory behind this new nanochromatography. The theory behind the single drop evaporation onto the dry surface and colloidal particles accumulation in the ring regions is well established and theoretical approaches have been developed [19,20]. Three major factors affect the formation of the CRE deposit: the radial outward flow, particle-surface interactions, and the reversed Marangoni flow, where the last one is relatively weak in the aqueous solutions and can be neglected [21]. The radial outward flow mainly depends upon the solvent evaporation flux, solution density, and the total evaporation time of the drying droplet, while the attraction/repulsion interactions govern the particles-substrate adsorption/desorption processes. These forces could be described by Derjaguin-Landau-Verwey-Overbeek theory (DLVO) that encompasses the interactions by the attractive van der Waals (LW) and repulsive electrostatic (EL) forces [22–24], and later the DLVO method was transposed into the extended DLVO theory (XDLVO) that introduced the new type of particle-particle interactions: the Lewis acid-base (AB) forces [25]. The XDLVO theory defines the stability of a colloidal solution as a function of Gibbs free energy interactions between particles summarizing repulsive EL, attractive LW, and donor-acceptor AB interactions as functions of particle separation and obtaining total free energy of interaction for a colloidal system. Typically, in aqueous media the donor-acceptor interactions are 10–100 times greater than EL and LW interactions stabilizing the colloidal suspension by hydration effects [26]. With the recent expansion of CRE-driven separation to small molecules, it becomes increasingly intriguing to relate the theory of coffee ring formation and particle-surface interaction to the separation process and ideally to resemble the classic plate and rate theories of chromatographic separation.

Herein, we have developed a theoretical framework to describe the CRE-driven separation process of small molecules, using SERS analysis of dimethylarsinic acid (DMA^{V}), dimethylmonothioarsinic acid ($DMMTA^{V}$), and dimethyldithioarsinic acid ($DMDTA^{V}$) on AuNF as an example. Our primary goal was to relate CRE-driven separation process to the conventional chromatographic theory during qualitative analysis of small molecules using CRE-based SERS. We created the theoretical approach for the CRE-based separation by encompassing the theory of the CRE, XDLVO, and traditional liquid chromatography [22]. We have applied the general chromatography theory for the development of the coffee ring effect providing that the radial outward flow in a drying droplet resembles the mobile phase of thin layer chromatography (TLC), gas chromatography (GC) and high pressure liquid chromatography (HPLC) systems. We further adapted the classic van Deemter equation for the quantification of radial flow and mass transfer parameters influencing separation efficiency by employing the XDLVO theory to consider arsenicals-AuNF surface interaction. We investigated both theoretically and experimentally the traveled distances of arsenicals across AuNF by changing the pH environment to find the optimal conditions for the separation. We then adjusted the radial outward flow for each compound obtained from the van Deemter curves for the individual arsenicals. By using this model, we predicted the traveled distances of arsenicals and evaluated the possibility of separation of unknown analytes by the coffee ring-SERS, demonstrating the successful adaptation of classic chromatographic theory to CRE-driven nanochromatography.

2. Experimental procedures

2.1. Materials and chemicals

Sodium dimethylarsenate 98% (DMA^{V}), NaOH, HCl, citric acid, sodium citrate dihydrate (Granular certified), (3-aminopropyl)trimethoxysilane (APTMS), glass microscope slides, weighing boats, and 25 ml glass vials were purchased from Fisher scientific Inc (Hampton, NH). The citrate buffer (pH = 3–7) was fabricated by mixing Citric acid and Sodium citrate. All solutions were prepared in deionized (DI) water (18.2 MΩ, Barnstead Nanopure Diamond).

2.2. Instrumentation

The Raman spectrometer was purchased from Jasko (NRS-4100), with a diode laser at 785 nm and average power of 33 mW. For optimizing resolving power, the 100 × optical lens focusing was used. A silicon wafer was employed to calibrate the Raman system at daily use and the Raman signal intensity at 520 cm^{-1} was monitored to check the reproducibility of the instrument. The SERS measurement parameters include the laser wavelength, 785 nm, exposure time, 4 s, and 1 time of exposure per measurement. The synthesis of thioarsenicals $DMMTA^{V}$ and $DMDTA^{V}$ and determination of their respective Raman spectra were performed in the previous reports [27,28].

The fabrication of AuNF was performed through the silanization of the glass substrates, followed by the deposition of nanoparticles onto the silanized surface (Figure S1) [29]. Immediately after the droplet contained 100 mg L^{-1} of arsenic ligands deposition onto the gold nanofilm, the droplet was freeze-dried, and the Raman spectra were collected. The adsorption of arsenic species onto the AuNF was carried out at pH = 3 and pH = 7, in the concentration range from 10^{-3} to 10^{-9} mol L^{-1}.

2.3. SERS fingerprint of arsenicals on the AuNF

The SERS vibrational fingerprints of DMA^{V}, $DMMTA^{V}$, and $DMDTA^{V}$ were measured individually by drying the liquid droplets (0.1 mol L^{-1} citrate buffer, pH = 4.0), followed by the Raman laser scan. The arsenical solutions were prepared by diluting the stock solution of 13.3 × 10^{-3} mol L^{-1} to 1.33 × 10^{-3} mol L^{-1} by addition of 0.1 mol L^{-1} citrate buffer (pH = 4.0). Typically, 2 μL of arsenic freshly prepared diluted solutions were dropped onto the AuNF, and SERS signals were obtained across the AuNF surface from the center to the edge regions. We have manipulated the evaporation time ranging from 35 to 2 min by completing the experiment in a vacuum chamber.

2.4. Adsorption of arsenicals to calculate the adsorption constants

The adsorption of analytes onto the nanoparticles in colloidal solution significantly differs from the adsorption onto nanofilms. To ensure the uniform adsorption (without the CRE), the freeze-drying

pretreatment were performed before SERS measurements once the 2 μL arsenicals buffer solution was placed onto the AuNF. The average SERS signal of arsenicals was acquired from the center to the edge of the dried deposit (n = 3). The SERS intensities for the quantitative analysis were normalized by the background correction.

2.5. Arsenicals speciation on the AuNFs

Arsenic speciation on AuNFs was performed by subsequent addition of individual arsenic standards, starting from DMA^V, followed by $DMMTA^V$, and $DMDTA^V$ to finally prepare a mixture of the three compounds. In contrast to the previous work [18], to simplify the model development we have not added surfactant sodium dodecyl sulfate (0.05% of SDS) that had the purpose to increase the radial outward flow by decreasing the surface tension of the deposited droplet. Standard solutions of arsenicals of 1.3×10^{-3} mol L^{-1} for each species were prepared in 0.1 mol L^{-1} citrate buffer (pH = 4.0. One drop (2 μL) of the solution was placed onto the AuNF surface, and the sessile droplet was left to evaporate under ambient conditions. In contrast to the previous two-ring formation of the droplet with SDS, we have observed only one ring formation. The three-phase contact line did not move during the evaporation of the sessile droplet. SERS measurements on all coffee ring drop stains were typically carried out from the center to the outer ring edge along the radius of the rings, and the sampling spots were performed with 200 μm increments according to the on-screen meter.

3. Results and discussion

3.1. Chromatographic theory for the separation of small molecules by CRE-SERS

We have incorporated the theories of CRE and XDLVO into the general chromatography theory (van Deemter equation) to develop the theoretical approach for the separation of small molecules by CRE-SERS analysis. The derived equations are shown here, and detailed information for the development of this theoretical framework can be found in Supporting Information. The velocity of radial outward flow (mobile phase) was calculated through the CRE theory, while the mass transfer for the arsenicals partition from the bulk to the nanofilm surface was characterized with the XDLVO theory. We extrapolated the XDLVO approach from its original nanoparticle-nanoparticle interaction forces to the small molecule-nanoparticle interactions. The mass transfer of arsenicals from the bulk to the AuNF surface depends upon the adsorption constant (K_{ad}), which is determined by the Gibbs free energy of the interaction between the AuNF and arsenicals, including the attractive interactions (van der Waals forces), the electrical double layer repulsive energy (EL) [30], and the polar surface interaction energy (AB). The second Fick's law was then applied for the adsorption of the arsenic ligand from the bulk to the nanofilm surface, where *the diffusion coefficient to stationary phase* (D_s) is related to K_{ad} through the retardation factor (R) [31,32]. By introducing the radial flow as the mobile phase and the adsorption constants as mass transfer parameters and assuming uniform porous distribution of the cavities (active sites) on the AuNF, we obtained the following modified van Deemter equation.

$$H = 2\varphi d_p + \frac{2\gamma D(m)}{u_R} + \left(\frac{wd^2}{D(m)} + \frac{j{d_f}^2}{\frac{\partial^2 C_s}{\partial C}\frac{\partial t}{\partial x^2} * (1 + K_{ad})} \right) u_R \quad (1)$$

where H is the plate height, φ is the nanoparticles shape, d_p is the diameter of AuNPs, $D(m)$ is the diffusion coefficient of the mobile phase; γ, w, j are constants, d_f is AuNF thickness.

Assuming that $D(m)$'s in liquid chromatography are relatively small in contrast to the gas chromatography, d_f is uniform, the equal speed of the arsenicals to be adsorbed on the AuNF surface, and the equal diffusion length of their adsorption path, after adding a time dependent variable depicting the mass transfer between the bulk and the AuNF surface we can simplify eq (1) into eq (2), realizing the adaption of classic chromatographic theory to the CRE-driven separation process. Detailed information for the development of this theoretical framework can be found in Supporting Information.

$$H = A + \frac{B}{u_R} + (C_m + k * C_S)u_R \quad (2)$$

where A is the eddy-diffusion parameter related to analytes movement through a non-ideal surface packing (m), B is the longitudinal diffusion coefficient of the eluting particles resulting in analytes dispersion across the mobile phase ($m^2 s^{-1}$), and C_m , C_S are the resistance to mass transfer coefficients of the analyte between mobile (C_m) and stationary phases (C_S) (s). The parameter k is a time dependent variable depicting the mass transfer between the bulk and the AuNF surface. The coefficient in front of C_S in classical van Deemter equation is equal to 1. In our system, providing that the evaporation time of a 2-μL droplet is 35 min, we would assume $k > 1$ at the earlier times ($t \approx 10$ min) when the system is heavily dominated by the mass transfer of the uniformly distributed analytes to the AuNF surface, while $k \approx 1$ for the later times (t = 20 min) when the system is balanced between the radial flow and the mass transfer processes.

3.2. Computational mechanism of arsenicals adsorption onto the AuNF surface

As the adsorption of arsenicals onto the AuNF surface controls the mass transfer from the bulk to the AuNF, we investigated the pH dependent arsenicals adsorption both theoretically and experimentally, allowing us to predict the pH influence on the traveled distances of arsenicals. We employed the QChem 4 software for the geometry optimization and energy calculations of arsenic-gold cluster complexes. Analyzing the gas phase optimized structures of arsenicals, we observed that negatively charged DMA^{V-}, $DMMTA^{V-}$, and $DMDTA^{V-}$ formed three bonds upon adsorbing onto the gold cluster in contrast to the neutral species that coordinated through a single interaction. To mimic the aqueous environment and to compensate for the solvation effects upon adsorption of negatively charged species onto the gold cluster, three molecules of water were added to each negatively charged arsenical. The energies of adsorption of neutrally charged arsenic ligand (DMA^V, $DMMTA^V$, $DMDTA^V$) were not affected by the solvation experiment with three water molecules, whereas the adsorption energies of negatively charged ligands (DMA^{V-}, $DMMTA^{V-}$ and $DMDTA^{V-}$) were considerably decreased after the solvent addition (Table 1). Thus, hydrogen bonding between the water and negatively charged ligands lowers the complexation energies.

The adsorption mechanism of thioarsenicals ($DMMTA^V$, $DMMTA^{V-}$ and $DMDTA^{V-}$) is similar to the adsorption of thiols and disulfides onto the AuNF. It starts with physisorption, with the H atom remaining within the hydroxyl group, and is followed by chemisorption leading to the

Table 1
The adsorption energies of arsenicals onto the AuNF surface.

Arsenical	ΔG_{tot} (DFT) (in vacuo) (kcal/mol)	ΔG_{tot} (DFT) (water) (kcal/mol)	ΔG_{tot} (Experimental) (kcal/mol)	K_{ad} (Experimental) (mol^{-1})
DMA^V-Au	−7.1	−7.1	−4.8	3.7×10^3
DMA^{V-}-Au	−31.5	−24.5	−5.2	7.0×10^3
$DMMTA^V$-Au	−19	−19	−6.1	3.0×10^4
$DMMTA^{V-}$-Au	−45	−30.4	−8.7	2.5×10^6
$DMDTA^{V-}$-Au	−40.5	−44.2	−11.4	1.5×10^8

breakage of the OH bond and formation of Au–O or Au–S bonds [33]. The adsorption mechanism included hybridization of p-like S orbitals with d-like Au orbitals producing both bonding and antibonding occupied orbitals. The process is well described by a model for the interaction of localized orbitals with narrow-band dispersive electron states at the bridge site between two surface Au atoms [34]. The Au–S bond is van der Waals dominated with lesser coordination and smaller directional input [35]. The neutral Au (0) $d^{10}s^0$ state dominates the nanofilm surface and the Au − Au bonding and reduces the covalent character of the Au − S bond. This is the cause of the directional change and the gold super exchange [36] leading to the S − Au adatom binding systems [37].

3.3. Theoretical and experimental gibbs free energy of Au-arsenicals complexation

The Langmuir isotherm was employed [38,39] for the calculation of the Gibbs free energy of arsenicals adsorption onto the AuNF surface (see Supporting Information for details). The structures of Au-arsenicals complexes, their SERS spectra, and corresponding adsorption isotherms are shown in Fig. 1, and the Gibbs free energies of complexation (DFT) of arsenical-Au clusters were calculated as shown below [40] and are summarized in Table 1.

$$\Delta G_{tot}\ (\text{gold} - \text{arsenical}) = \Delta G_{tot}\ (\text{gold} - \text{arsenical}) - \Delta G_{tot}(\text{gold}) - \Delta G_{tot}\ (\text{arsenical}) \quad (3)$$

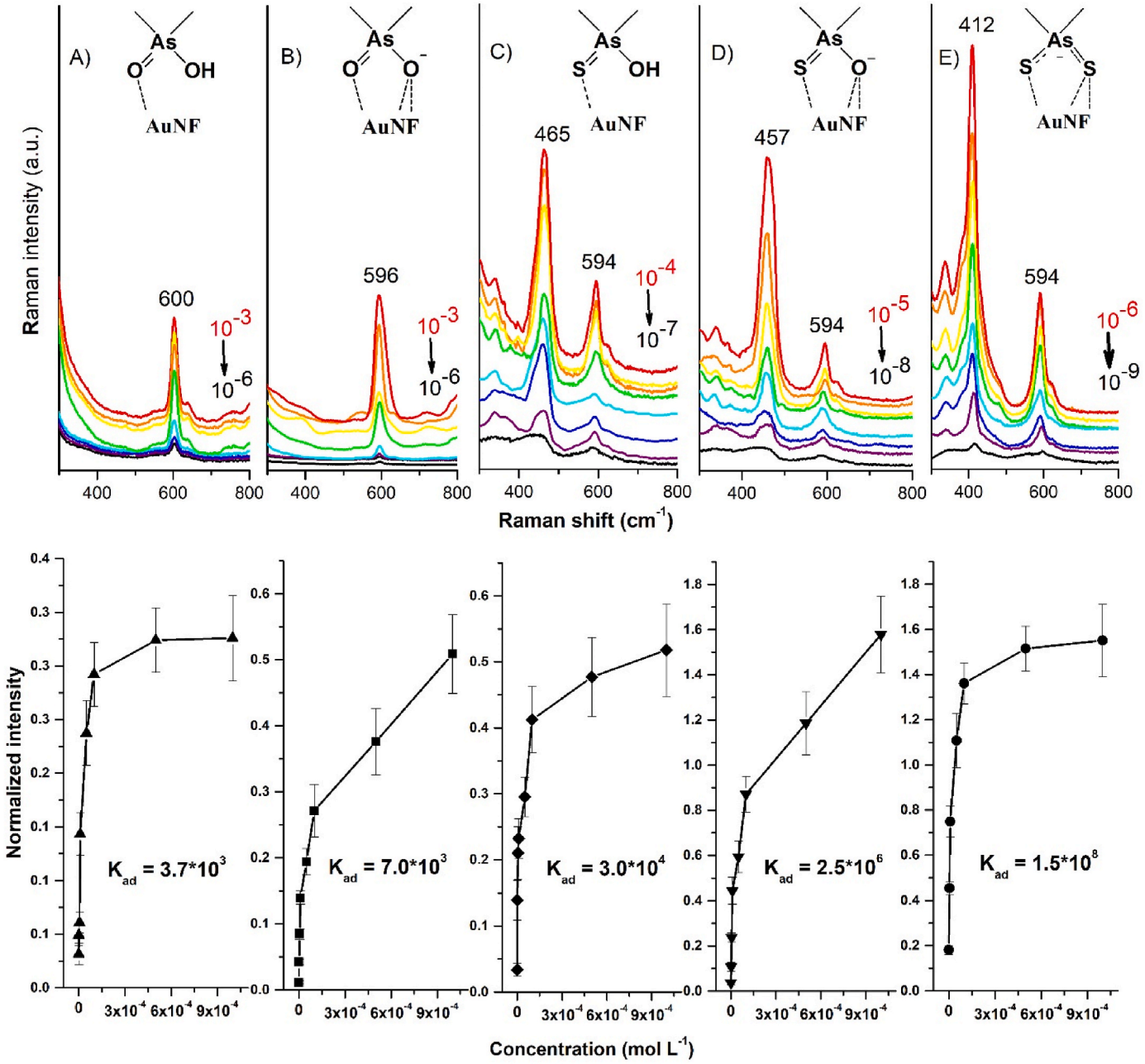

Fig. 1. The adsorption isotherms of arsenicals upon complexing with the AuNF and the corresponding SERS spectra of A) protonated dimethylarsinic acid DMA^V, 600 cm^{-1} and B) deprotonated dimethylarsinic acid DMA^{V-}, 596 cm^{-1} (the As − C symmetric stretching); C) dimethylmonothioarsinic acid $DMMTA^V$, 465 cm^{-1}, and D) deprotonated dimethylmonothioarsinic acid $DMMTA^{V-}$, 457 cm^{-1} (the As═S stretching); E) deprotonated dimethyldithioarsinic acid $DMDTA^V$, 412 cm^{-1} (the As ÷ S delocalized stretching).

The adsorption of arsenicals onto the AuNF surface is pH dependent. The negatively charged arsenic-Au complexes (DMA^{V-}-Au, $DMMTA^{V-}$-Au, $DMDTA^{V-}$-Au) demonstrate the lower Gibbs free energy and, consequently, the higher binding affinity to the AuNF in contrast to the neutral adsorbates (DMA^{V}-Au, $DMMTA^{V}$-Au). The calculated energies were lower than the literature data for the similar sulfur containing compounds mainly because of the computational limitations; only three molecules of water were employed for the solvation simulation of the arsenicals-AuNF complexes. However, even with the limited solvation, the experimental data correlate with the theoretical values. Considering the experimental data, it is clear that the adsorption of the sulfur containing arsenicals ($DMMTA^{V}$-Au, $DMMTA^{V-}$-Au, $DMDTA^{V-}$-Au) regardless of the molecular charge was chemisorption like process in agreement with the literature data for the thiols and sulfides chemisorption adsorption onto the AuNF surface (6–14 kcal), whereas oxygen containing arsenicals (DMA^{V}-Au, DMA^{V-}-Au) demonstrated physisorption (with Gibbs free energies less than 6 kcal) [41,42]. The binding capacity of negatively charged thiolates ($DMDTA^{V-}$) is generally higher than that of neutral thiones ($DMMTA^{V}$) [33]. The general trend for the adsorption of arsenicals from the highest to the lowest adsorption values is the following: $DMDTA^{V-}$-Au > $DMMTA^{V-}$-Au > $DMMTA^{V}$-Au > DMA^{V-}-Au > DMA^{V}-Au.

3.4. Travel distance of arsenicals under different pHs

The travel distances of arsenicals were estimated in the pH range from 3 to 7 as shown in Table 2, where a relative retention, t_R (compound))/t_R (solvent), was defined and used for describing the travel distances of each analyte. To trace DMA^{V} we have recorded the SERS signals for the As − C stretching at 600 cm^{-1} for neutral, and 598 cm^{-1} for the deprotonated forms across the CRE stain. In the pH range from 3 to 5, the neutral form of DMA^{V} (pKa = 6.20) traveled a longer distance from the center to the edge regions of the drying droplet, however, as the pH increases, the length of the movement decreased, which can be attributed to the stronger interactions between DMA^{V-} and citrate anions through the hydrogen bonding resembling As^{III}–AuNF complexation [43]. Similarly, $DMMTA^{V}$ (the As═S stretching, 469 cm^{-1} for neutral – 457 cm^{-1} for the deprotonated forms) having pKa of 3.5 covered longer distance in contrast to the deprotonated compound. Once the pH increases, the $DMMTA^{V}$ becomes more ionic decreasing its Gibbs free energy of adsorption (Table 1) and substituting the citrate onto the AuNF surface. Considering $DMDTA^{V}$'s (the As ÷ S stretching, 412 cm^{-1}, pKa = 2.25) traveled distance it was not considerably affected by the pH changes. Regarding the higher adsorption energy of $DMDTA^{V}$ onto the AuNF surface than those of DMA^{V} and $DMMTA^{V}$, this arsenical was immediately adsorbed onto the AuNF surface, representing the constant SERS signal across all regions. Overall, it is implied that the higher attraction of the arsenicals to the surface, the shorter migration distance and larger the Raman shift.

3.5. Optimizing parameters for the derived van deemter equation: pH and radial flow velocity

We started the separation optimization by selectively tuning the pH of the mobile phase to maximize the difference in traveled distances of each arsenical. Thus, the retention factor (k) normalized by the mobile phase front and the selectivity factor (α) were plotted against the pH to obtain the pH windows for each pair of arsenicals as shown in Fig. 2A and Fig. 2B respectively. The highest selectivity for DMA^{V}/$DMMTA^{V}$ and DMA^{V}/$DMDTA^{V}$ was achieved at pH = 4.0.

To further optimize the separation capacity of the developed method we have calculated the optimal mobile phase rate by employing the vacuum chamber for the adjustment of the sessile droplet evaporation rate, considering the radial outward flow is proportional to the velocity of evaporation (Figure S3). The graph of the Height Equivalent to a Theoretical Plate (HETP) vs the radial flow velocity was constructed in Fig. 2C. Analyzing the van Deemter curves of the individual arsenicals it is seen that the increase of the mobile phase rate at the higher evaporation times significantly affects the HETP of DMA^{V}, in contrast to that of thioarsenicals $DMMTA^{V}$ and $DMDTA^{V}$. This could be because of the difference in the retention factors of DMA^{V} and thioarsenicals. At lower speeds of the mobile phase, DMA^{V} is much more influenced by the radial movement resulting in the minimum of the HETP at 23.5 min. Interestingly, that radial flow considerably affects HETP's of thioarsenicals, only at the fastest rates providing the minimum of HETP at 15.2 and 7.4 for $DMMTA^{V}$ and $DMDTA^{V}$, respectively. The optimal velocity of the radial flow was computed to be 15.4 min. The extended calculations of the HETP and arsenicals' travel distances are presented in Table S1.

Table 2
The pH dependent traveled distances of arsenicals on the AuNF (τ_{evap} =35 min).

Relative retention, $\frac{t_{R(compound)}}{t_{R(solvent)}}$				$t_{R\ (solvent)}$, mm
pH	DMA^{V}(As–C)	$DMMTA^{V}$(As═S)	$DMDTA^{V}$(As ÷ S)	H_2O/buffer
3	0.81 ± 0.09	0.40 ± 0.03	0.46 ± 0.04	6.20 ± 0.74
4	0.81 ± 0.07	0.39 ± 0.03	0.47 ± 0.03	
5	0.65 ± 0.08	0.37 ± 0.03	0.47 ± 0.05	
6	0.57 ± 0.08	0.36 ± 0.02	0.47 ± 0.03	
7	0.50 ± 0.08	0.35 ± 0.02	0.48 ± 0.02	

3.6. Separation of arsenicals in CRE-SERS analysis

The mixture of DMA^{V}, $DMMTA^{V}$, and $DMDTA^{V}$ was analyzed using CRE-SERS at the optimized conditions for the separation at pH = 4.0 and the radial flow velocity corresponding to an evaporation time of 15.4 min (Figure S3). The CRE was observed for DMA^{V} and $DMDTA^{V}$ resulting in the higher SERS intensity in the ring region. $DMMTA^{V}$'s SERS signals were similar in the middle and ring regions and the CRE formation was not so evident as for DMA^{V} and $DMDTA^{V}$.

The differences in traveled distances of the arsenicals showed their separation. From Fig. 3, DMA^{V} was found in the edge region of the CRE, whereas the mixture of $DMMTA^{V}$ and $DMDTA^{V}$ was detected in the middle region following $DMDTA^{V}$ in the center region respectively. Due to the presence of S in the thioarsenicals molecules, $DMMTA^{V}$ and $DMDTA^{V}$ have a higher affinity to the AuNF in contrast to DMA^{V} that lacks sulfur atoms. Thus, we hypothesize that in contrast to thioarsenicals, DMA^{V} was not able to substitute citrate onto the AuNF surface and traveled a longer distance reaching the edge region. Moreover, the increase of DMA^{V}'s As − O stretching SERS intensity was not observed, however the As − C asymmetrical stretching (599 cm^{-1}) mode was enhanced. Since DMA^{V} could not bind to the AuNF surface, this could happen by substituting the citrate onto the AuNF surface. This explanation for a longer traveled distance of DMA^{V} could be pKa based: Having pKa of 6.2, DMA^{V} at pH = 4.0 is mostly neutral in contrast to $DMMTA^{V}$ (pKa = 4.37) and $DMDTA^{V}$ (pKa = 2.25) molecules, that bear a negative charge in addition to sulfur atoms and, consequently interact stronger with the AuNF surface resulting in the shorter traveled distances than that of DMA^{V}. The final location of each arsenical after the CRE separation is shown in Figure S4. The CRE regions and the process of the sessile droplet evaporation are presented in Video S1.

Supplementary data related to this article can be found at https://doi.org/10.1016/j.talanta.2022.123688.

The resolution calculation of each pair of compounds was summarized in Table S2 and illustrated in Figure S5. For DMA^{V}/$DMMTA^{V}$ and DMA^{V}/$DMDTA^{V}$ the peak resolution was found to be 1.5 which is the minimum method resolution that allowed the proper peak identification. However, for $DMMTA^{V}$/$DMDTA^{V}$ the resolution accounted only for 0.6 at optimized separation conditions. Even though the peak resolution was not enough to identify components based on their retention time, SERS provides a unique advantage by providing the unique fingerprint and allowing the identification of thioarsenicals based on their arsenic sulfur vibrations: $DMDTA^{V}$ (As ÷ S stretching at 412 cm^{-1}) and

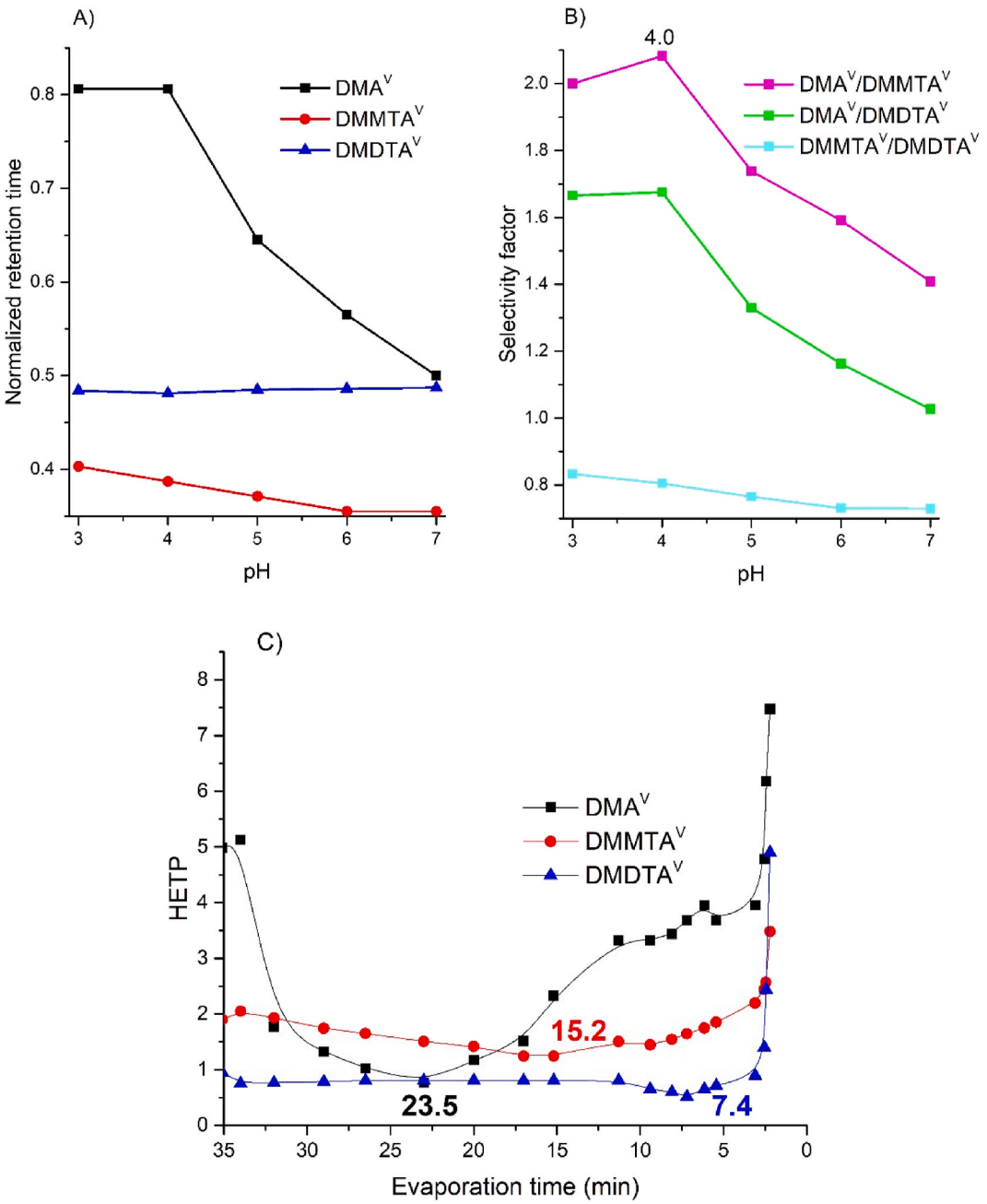

Fig. 2. A) retention factor (k) and B) the selectivity factor (α) for CRE-driven separation of arsenicals under different pHs; C) HETP curves of individual arsenicals obtained from the modified van Deemter equation [44] to calculate the optimal mobile phase velocity rate for DMA^V, DMMTA^V, and DMDTA^V.

DMMTA^V (As═S stretching at 465 cm^{-1}).

3.7. General application of developed theoretical framework to CRE-SERS of small molecules

The developed theory can be used to predict the traveled distances of analytes by the pH and radial flow, expanding its applications for the CRE-driven separation of small molecules in general. As pH plays a crucial role in mass transport of compounds to the nanofilm surface, the pKa's of analytes (if unknown) needs to be calculated, e.g., by Marvin Sketch software that was deemed reliable here, followed by the optimization of pH to adjust the retention time and selectivity factor. Normally, as pH increases exceeding the pKa of an analyte, the adsorption constant of the species increases and the Gibbs free energy becomes more negative, resulting in the increased retardation factor that magnifies the diffusion coefficient and sorption of analytes (diffusion flux) onto the surface, thus the increased mass transfer from the bulk to the surface. The charged molecules usually travel shorter distances than the neutral ones do. The radial flow can also be adjusted to guide the molecule into the specific region of the coffee ring, this could be tuned by manipulating the atmospheric pressure evaporation of the sessile droplet. The lower the atmospheric pressure, the higher the evaporation rate and thus the higher the radial outward flow, resulting in the increase of the traveled distances.

To selectively apply this theory to small molecules, the following questions need to be considered: 1) What are the differences in molecular structures of target analytes that may trigger different interactions of these analytes with the negatively charged gold nanoparticles? and 2) What types of interactions do the target molecules have with the gold nanofilm (electrostatic, van der Waals, or donor-acceptor)? The final

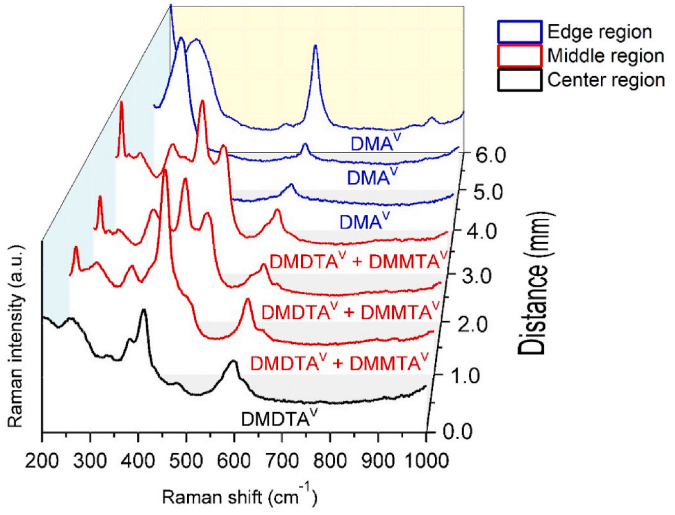

Fig. 3. The CRE of DMA^V, DMMTA^V, DMDTA^V onto the AuNF at the optimized separation conditions (pH = 4.0, u_R = 15.4 min).

locations of analytes after the solvent evaporation could be expected in 1) the center region, where a molecule of interest is not significantly affected by the radial outward flow, because it is hydrophobic or has a very high affinity to the AuNF surface through electrostatic attraction (positively charged molecules) or donor-acceptor interactions (like DMDTA^{V-} and DMMTA^{V-} here); 2) the middle region, where a compound is affected by the radial flow as it could be a neutral molecule that has relatively high AuNF surface attraction (like DMMTA^V and DMA^{V-}); or 3) the edge region, where an analyte is considerably affected by the radial flow as it might have the predominant neutral charge and a hydrophilic character (like DMA^V). For the analytes that might not be completely separated by the CRE, SERS provides an additional advantage to identify the species through fingerprint Raman shifts.

One of the key advantages of the developed method is the minimal sample pretreatment allowing the complex samples to be analyzed without extensive sample preparation, enabling rapid field analysis. Also, the substrate surface charge can be easily modified to anchor negatively charged analytes in the specific CRE regions by fabricating positively charged AuNF and vice versa. The analytes-AuNF electrostatic attraction results in the increase of analytes adsorption, thus, the further enhancements of the SERS output signal and method sensitivity. Besides, thanks to the small substrate size (1.5 × 1.5 cm^2), the AuNF is quite compact and versatile, it might be placed into the gas chamber, oven, etc. Also, the analytes' migration distances can be manipulated through the adjustments of the radial outward flow by placing a substrate into a vacuum chamber.

The major disadvantage of the developed method is the homogeneity issue of the substrate surface. The nonuniform AuNPs deposition results in the unstable SERS signals. There have been challenges with SERS method for quantitative analysis, as SERS scanning varies significantly with locations (e.g., due to non-homogeneous nanoparticles distribution onto the surface), especially when CRE-driven separation process is involved. Although our previous work using Ag or Au nanofilms for CRE-based SERS analysis of arsenicals suggested that the formation of coffee ring was relatively consistent during droplet evaporation and the SERS spectrum and signal at the same location could be reproducible in different batches of experiments [17], the spatial nonuniformity of AuNPs deposition and thus SERS signals remains a crucial factor limiting CRE-SERS for quantitative analysis. Another drawback is that the gradient elution is limited to the 0.05% (v/v) concentration of organic phase in the water droplet. The further addition of organic solvents greatly lowers the water surface tension disturbing the three-phase contact line and resulting in the uncontrolled drop spreading across the AuNF surface.

The CRE driven separations might be further improved by adjusting the following factors: the increase of the nanofilm length (L) results in the resolution increase by the factor of $\sqrt{L}$; the addition of surfactants (0.05%) promotes the formation of two rings system, which allows visualizing the two-rings CRE system: the inner (water-based) and the outer (surfactant-based) rings. Nonpolar analytes tend to be carried away by surfactant and ended up on the outer ring, while the polar compounds cover most of the inner ring. To describe the two-ring system, however, further adjustments of the modified van Deemter equation are needed.

4. Conclusions

A theoretical approach based on the combination of the CRE-driven separation and SERS detection on AuNFs has been developed for the speciation of small molecules. Considering the major factors affecting the formation of the CRE deposit, i.e. radial outward flow, analyte-AuNFs interactions and Marangoni flow, the traditional chromatographic theory was adapted to derive a modified van Deemter equation for the CRE-driven separation, by combining the CRE theory for the radial flow and the XDLVO theory for the analyte-surface interactions. Through manipulating pH and the radial flow to find optimal conditions for the separation of DMA^V, DMMTA^V, and DMDTA^V, we demonstrated that the theoretical model could predict the travel distances of small molecules during the formation of the CRE deposit based on different affinity of analytes with the AuNFs. This theoretical framework adopts a unified approach for both the conventional chromatographic techniques (e.g., GC and HPLC) and the CRE-based nanochromatography which employs a stationary phase on the nanometer scale to enable the separation at a very short distance (~5 mm). CRE-SERS analysis requires minimal sample pretreatment and allows for nondestructive and simultaneous detection of multiple species, thus presenting an alternative approach for potential in situ detection of fragile compounds.

Credit author statement

Valery Liamtsau: design and conduct experiments, interpret data, write article **Guangliang Liu**: design experiment, interpret data, write article **Alexander N. Morozov**: conduct computational component of the research, interpret data **Alexander M. Mebel**: design computational component of the research, interpret data **Yong Cai**: design and interpret data, write article

Declaration of competing interest

The authors declare that they have no known competing financial interests or personal relationships that could have appeared to influence the work reported in this paper.

Acknowledgments

Authors gratefully acknowledge NSF programs (ECS1905239) for the support of the work. Valery Liamtsau acknowledges the Florida International University for financial support of his dissertation research. This is contribution number 1123 from the Southeast Environmental Research Center in the Institute of Water & Environment at Florida International University.

Appendix A. Supplementary data

Supplementary data to this article can be found online at https://doi.org/10.1016/j.talanta.2022.123688.

References

[1] R.D. Deegan, et al., Capillary flow as the cause of ring stains from dried liquid drops, Nature 389 (6653) (1997) 827.
[2] J.-H. Kim, et al., Evaporation of water droplets on polymer surfaces, Langmuir 23 (11) (2007) 6163–6169.
[3] J.-Y. Jung, Y.W. Kim, J.Y. Yoo, Behavior of particles in an evaporating didisperse colloid droplet on a hydrophilic surface, Anal. Chem. 81 (19) (2009) 8256–8259.
[4] V.R. Dugyala, M.G. Basavaraj, Evaporation of sessile drops containing colloidal rods: coffee-ring and order–disorder transition, J. Phys. Chem. B 119 (9) (2015) 3860–3867.
[5] J.-B. Hu, Y.-C. Chen, P.L. Urban, Coffee-ring effects in laser desorption/ionization mass spectrometry, Anal. Chim. Acta 766 (2013) 77–82.
[6] R. Hara, et al., Surface-enhanced Raman spectroscopy using a coffee-ring-type three-dimensional silver nanostructure, RSC Adv. 5 (2) (2015) 1378–1384.
[7] J.B. Miller, et al., Phase separation and the 'coffee-ring'effect in polymer–nanocrystal mixtures, Soft Matter 10 (11) (2014) 1665–1675.
[8] V. Kopecký Jr., V. Baumruk, Structure of the ring in drop coating deposited proteins and its implication for Raman spectroscopy of biomolecules, Vib. Spectrosc. 42 (2) (2006) 184–187.
[9] J. Xu, et al., Facile detection of polycyclic aromatic hydrocarbons by a surface-enhanced Raman scattering sensor based on the Au coffee ring effect, ACS Appl. Mater. Interfaces 6 (9) (2014) 6891–6897.
[10] D. Zhang, et al., Raman detection of proteomic analytes, Anal. Chem. 75 (21) (2003) 5703–5709.
[11] T.-S. Wong, et al., Nanochromatography driven by the coffee ring effect, Anal. Chem. 83 (6) (2011) 1871–1873.
[12] S. Choi, et al., Coffee-ring effect-based three dimensional patterning of micro/nanoparticle assembly with a single droplet, Langmuir 26 (14) (2010) 11690–11698.
[13] K.A. Baldwin, et al., Monolith formation and ring-stain suppression in low-pressure evaporation of poly (ethylene oxide) droplets, J. Fluid Mech. 695 (2012) 321–329.
[14] K. Gracie, et al., Simultaneous detection and quantification of three bacterial meningitis pathogens by SERS, Chem. Sci. 5 (3) (2014) 1030–1040.
[15] D. Karthigeyan, et al., SERS and MD simulation studies of a kinase inhibitor demonstrate the emergence of a potential drug discovery tool, Proc. Natl. Acad. Sci. USA 111 (29) (2014) 10416–10421.
[16] W. Wang, et al., Coffee-ring effect-based simultaneous SERS substrate fabrication and analyte enrichment for trace analysis, Nanoscale 6 (16) (2014) 9588–9593.
[17] M. Yang, et al., Arsenic speciation on silver nanofilms by surface-enhanced Raman spectroscopy, Anal. Chem. 91 (13) (2019) 8280–8288.
[18] V. Liamtsau, Y. Cai, Application of nanofilms for arsenic speciation using surface-enhanced Raman spectroscopy (SERS), in: Environmental Arsenic in a Changing World: Proceedings of the 7th International Congress and Exhibition on Arsenic in the Environment, CRC Press, Beijing, PR China, 2019. *AS 2018), July 1-6, 2018*.
[19] F. Boulogne, F. Ingremeau, H.A. Stone, Coffee-stain growth dynamics on dry and wet surfaces, J. Phys. Condens. Matter 29 (7) (2016), 074001.
[20] R. Bhardwaj, X. Fang, D. Attinger, Pattern formation during the evaporation of a colloidal nanoliter drop: a numerical and experimental study, New J. Phys. 11 (7) (2009), 075020.
[21] X. Xu, J. Luo, Marangoni flow in an evaporating water droplet, Appl. Phys. Lett. 91 (12) (2007), 124102.
[22] R. Bhardwaj, et al., Self-assembly of colloidal particles from evaporating droplets: role of DLVO interactions and proposition of a phase diagram, Langmuir 26 (11) (2010) 7833–7842.
[23] Z. Adamczyk, P. Weroński, Application of the DLVO theory for particle deposition problems, Adv. Colloid Interface Sci. 83 (1–3) (1999) 137–226.
[24] V.n.L. Morales, et al., Surfactant-mediated control of colloid pattern assembly and attachment strength in evaporating droplets, Langmuir 29 (6) (2013) 1831–1840.
[25] E.M. Hoek, G.K. Agarwal, Extended DLVO interactions between spherical particles and rough surfaces, J. Colloid Interface Sci. 298 (1) (2006) 50–58.
[26] D. Grasso, et al., A review of non-DLVO interactions in environmental colloidal systems, Rev. Environ. Sci. Biotechnol. 1 (1) (2002) 17–38.
[27] W.R. Cullen, et al., Methylated and thiolated arsenic species for environmental and health research—a review on synthesis and characterization, J. Environ. Sci. 49 (2016) 7–27.
[28] K.T. Suzuki, et al., Dimethylthioarsenicals as arsenic metabolites and their chemical preparations, Chem. Res. Toxicol. 17 (7) (2004) 914–921.
[29] A.F. Scarpettini, A.V. Bragas, Coverage and aggregation of gold nanoparticles on silanized glasses, Langmuir 26 (20) (2010) 15948–15953.
[30] C. Van Oss, R. Giese, P.M. Costanzo, DLVO and non-DLVO interactions in hectorite, Clay Clay Miner. 38 (2) (1990) 151–159.
[31] K.C. Van Rees, et al., Evaluation of laboratory techniques for measuring diffusion coefficients in sediments, Environ. Sci. Technol. 25 (9) (1991) 1605–1611.
[32] A. Matos, et al., Retardation factors and the dispersion-diffusion coefficients of Zn, Cd, Cu, and Pb in soils from Vicosa-MG, Brazil, Transactions of the ASAE 42 (4) (1999) 903.
[33] S.M. Ansar, et al., Determination of the binding affinity, packing, and conformation of thiolate and thione ligands on gold nanoparticles, J. Phys. Chem. C 115 (3) (2010) 653–660.
[34] R. Di Felice, A. Selloni, E. Molinari, DFT study of cysteine adsorption on Au (111), J. Phys. Chem. B 107 (5) (2003) 1151–1156.
[35] J.R. Reimers, et al., Competition of van der Waals and chemical forces on gold–sulfur surfaces and nanoparticles, Nat. Rev. Chem 1 (2) (2017), 0017.
[36] J.R. Reimers, et al., Gold Surfaces and Nanoparticles Are Protected by Au (0)–thiyl Species and Are Destroyed when Au (I)–thiolates Form, Proceedings of the National Academy of Sciences, 2016, 201600472.
[37] L. Costelle, et al., Binding of deposited gold clusters to thiol self-assembled monolayers on Au (111) surfaces, Appl. Phys. Lett. 98 (4) (2011), 043107.
[38] Y. Liu, Is the free energy change of adsorption correctly calculated? J. Chem. Eng. Data 54 (7) (2009) 1981–1985.
[39] J. Kubackova, et al., Sensitive surface-enhanced Raman spectroscopy (SERS) detection of organochlorine pesticides by alkyl dithiol-functionalized metal nanoparticles-induced plasmonic hot spots, Anal. Chem. 87 (1) (2014) 663–669.
[40] H. Al-Johani, et al., The structure and binding mode of citrate in the stabilization of gold nanoparticles, Nat. Chem. 9 (9) (2017) 890.
[41] L.L. Rouhana, M.D. Moussallem, J.B. Schlenoff, Adsorption of short-chain thiols and disulfides onto gold under defined mass transport conditions: coverage, kinetics, and mechanism, J. Am. Chem. Soc. 133 (40) (2011) 16080–16091.
[42] D.J. Lavrich, et al., Physisorption and chemisorption of alkanethiols and alkyl sulfides on Au (111), J. Phys. Chem. B 102 (18) (1998) 3456–3465.
[43] L. Gong, et al., Colorimetric aggregation assay for arsenic (III) using gold nanoparticles, Microchim. Acta 184 (4) (2017) 1185–1190.
[44] H.W. Moody, The evaluation of the parameters in the van Deemter equation, J. Chem. Educ. 59 (4) (1982) 290.